THE JOURNAL OF PHYSICAL CHEMISTRY A
A JOURNAL OF THE AMERICAN CHEMICAL SOCIETY

pubs.acs.org/JPCA

Article

Magnetic and Thermodynamic Computations for Supramolecular Assemblies between a Cr(III) and Fe(III) Single-Ion Magnet and an Fe(II) Spin-Crossover Complex

Angel Albavera-Mata, Shuanglong Liu, Hai-Ping Cheng, Richard G. Hennig,* and S. B. Trickey*

Cite This: *J. Phys. Chem. A* 2024, 128, 10929−10935

Read Online

ACCESS | Metrics & More | Article Recommendations | Supporting Information

ABSTRACT: Experimental results on two supramolecular complexes in which a Cr^{III} or Fe^{III} d-orbital single-ion magnet center is embedded between a pair of Fe^{II} spin-crossover moieties make those two complexes interesting as possible candidates for use in quantum information technologies. We report detailed computational results for their structure and electronic properties and use the resulting data to parametrize a spin Hamiltonian that facilitates comparison with experimental results and their interpretation. Consistent with experimental results on decoherence in $[Fe(ox)_3]@[Fe_2L_3]^+$, we find it to be easy-plane type while the $[Cr(ox)_3]@[Fe_2L_3]^+$ system is easy-axis type.

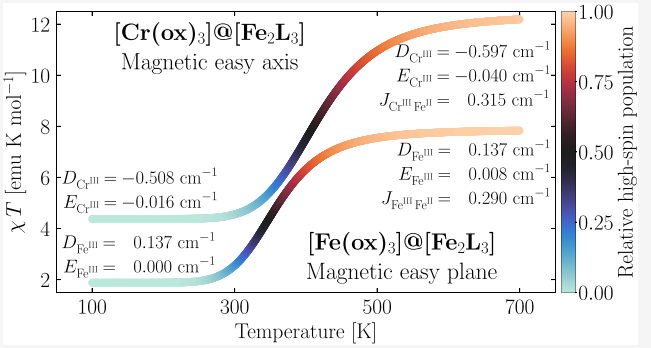

INTRODUCTION

Development of magnetic material frameworks for quantum information technologies at nanoscale requires accessible long-term stability of molecular magnetic systems to serve as the required building blocks for scalable communication and information storage.[1−12] Use of simple single-ion magnets (SIMs) in mononuclear f-block metal complexes is one potential solution on account of their long coherence times and useful magnetic anisotropy that might be manipulated through suitable local coordination environments.[13,14] Those features are in contrast with poly-nuclear clusters with d-block metal centers.[15−19] However, the large-scale use of f-block metals would have some notable disadvantages, among them being scarcity relative to first-row d-block metals. Moreover, the early promise of being able to synthesize SIMs based on a transition metal core that has competitive anisotropy and slow magnetic relaxation[20] pushed the mainstream interest toward synthesizing ionic magnets with Cr, Mn, Fe, Co, and Ni.[21]

Materials designed for eventual technological applicability also would have the capability to tune the interactions between magnetic units. This can be achieved by bridging the SIMs through linker chains, by creating one- two- or three-dimensional arrays,[22−29] by confinement in porous materials,[30−34] or by adsorption on appropriate surfaces.[35−38] Use of transition metals also allows for the creation of strongly coupled spin interactions across metallic centers that may be exploited not only for information storage but also for signal transfer.[39−43] This last property is of particular interest in opening a niche of opportunity for supramolecular chemistry.

In this context, the ideal supramolecular assemblies constitute species that are responsive to some external stimulus, for example, pressure, temperature, light, or magnetic field, and, at the same time, enhance, or at least do not diminish, the properties of the isolated SIM. To our knowledge, three such molecules have been reported,[44−46] namely, $[Cr(ox)_3]@[Fe_2L_3]^+$, $[Fe(ox)_3]@[Fe_2L_3]^+$, and $[Fe(anilate)_3]@[Fe_2L_3]^+$. The first two host a Cr^{III} or Fe^{III} trisoxalate (ox), while the third has an Fe^{III} trianilate magnetic guest, each inside an Fe^{II} spin-crossover complex with three ligands L = 3,3′-bis(3-(pyridin-2-yl)-1*H*-pyrazol-5-yl)-1,1′-biphenyl.

Regarding the spin-switching properties of the chelates, transition temperatures $T_{1/2}$ of approximately 200 K and over 250 K are reported for $[Cr(ox)_3]@[Fe_2L_3]^+$ and $[Fe(ox)_3]@[Fe_2L_3]^+$, respectively. In contrast, $[Fe(anilate)_3]@[Fe_2L_3]^+$ exhibits a stepped transition starting at 250 K for the first Fe^{II} and around 300 K for the second Fe^{II} ion. We defer the study of that system because of its qualitatively different characteristics and focus here on the first two. Notably, they also can be brought to a low-temperature metastable high-spin (HS) state through light-induced excited spin-state trapping.

Received: October 3, 2024
Revised: November 18, 2024
Accepted: November 25, 2024
Published: December 6, 2024

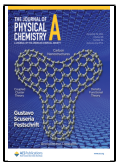

https://doi.org/10.1021/acs.jpca.4c06723
J. Phys. Chem. A 2024, 128, 10929−10935

The chemical and physical traits of the first two coordination complexes, namely, significant coherence time for the Cr^{III} moiety or its suppression for the Fe^{III} moiety, high transition temperature, and encapsulation of the ionic magnet, make them attractive as candidate precursors for quantum information materials. In this work, we investigate the thermodynamic stability of those two helicates by computing the thermal evolution of the magnetic susceptibility for the parallel and antiparallel spin interactions between the spin-switching centers of the complexes. From the calculated total energies for various magnetic configurations, we fit a model spin Hamiltonian that includes the dipolar spin−spin interactions and spin−orbit coupling in the zero-field splitting (ZFS) parameters and compare the computed results with experimental values.[47−54] Our results provide evidence that antiparallel coupling between the magnetic and spin-switching centers is energetically favored in both complexes, with the Cr^{III} ion system having a magnetic easy axis, whereas the Fe^{III} ion system has a magnetic easy plane instead.

COMPUTATIONAL DETAILS

All of our electronic structure results are from Kohn−Sham density functional theory calculations done in VASP 6.3[55] under periodic boundary conditions with the supramolecular complex placed inside an orthorhombic box having at least 10 Å of vacuum. We used the Perdew−Burke−Ernzerhof (PBE) density functional approximation,[56,57] both without and with long-range dispersion corrections, using the Becke−Johnson damping function.[58] Both types of calculations were performed with the set of projector augmented wave pseudopotentials listed in Table 1. Effective Hubbard-U_{eff} values were calculated

Table 1. Element and Valence Electrons, Z_{val}, of the Projector Augmented Wave Potentials

element	Z_{val}	potential
H	1	PAW_PBE H 15Jun2001
B	3	PAW_PBE B 06Sep2000
C	4	PAW_PBE C 08Apr2002
N	5	PAW_PBE N 08Apr2002
O	6	PAW_PBE O 08Apr2002
F	7	PAW_PBE F 08Apr2002
Cr	14	PAW_PBE Cr_sv 23Jul2007
Fe	16	PAW_PBE Fe_sv 23Jul2007

using linear response[59] on the mean-value ensemble spin state.[60] The results are U_{eff} = 1.96, 1.24, and 1.88 eV for Fe^{II}, Cr^{III}, and Fe^{III}, respectively.

In VASP, the plane wave kinetic energy cutoff was set to 600 eV, with an auxiliary support grid used for the augmentation charge evaluation. The nonspherical corrections to the electron density gradients were activated, and the accurate precision tolerance was selected. The threshold for the electronic steps was set to 10^{-8} eV for the calculation of energy differences and harmonic frequencies, along with Gaussian smearing of 10^{-2} eV, and with the projection operators evaluated in reciprocal space. Geometry relaxations started from the experimental structures[44,45] and were carried out until forces were smaller in magnitude than 10^{-3} eV Å^{-1}.

The thermal variation of the magnetic susceptibility can be approximated by means of the effective magnetic moment using the total orbital momentum, L, and total spin angular momentum, S, through $\mu_{L,S} = \sqrt{4S(S+1) + L(L+1)}\,\mu_B$, where μ_B = 9.274 J T^{-1} is the Bohr magneton. For that, we expressed $\mu_{L,S}$ as an ensemble average between S and L for the low- and high-spin states weighted by the relative high-spin population, α_{HS}, for a given temperature and considering an ideal solution model.[61] In it, the Gibbs free energy of the noninteracting systems is

$$G = (1 - \alpha_{HS})G_{LS} + \alpha_{HS}G_{HS} - TS_{mix} \quad (1)$$

The ideal entropy of mixing is $S_{mix} = -N_A k_B(\alpha_{HS}\ln[\alpha_{HS}] + (1 - \alpha_{HS})\ln[1 - \alpha_{HS}])$, where N_A is Avogadro's number and k_B is Boltzmann's constant. The equilibrium condition $(\partial G/\partial\alpha_{HS})_{T,P} = 0$ applied to eq 1 then determines the transition temperature $T_{1/2} = \Delta H/\Delta S$ for $\alpha_{HS} = 1/2$, with ΔH and ΔS being the enthalpy and entropy difference, respectively, between the high- and low-spin molecular states. Those differences are expressed in terms of electronic, rotational, translational, and vibrational contributions as

$$\Delta H = \Delta E_{HL} + \Delta E_{vib} + P\Delta V \quad (2)$$

$$\Delta S = \Delta S_{ele} + \Delta S_{rot} + \Delta S_{tra} + \Delta S_{vib} \quad (3)$$

Here, ΔE_{HL} is the adiabatic spin conversion energy $\Delta E_{HL} = E_{HS} - E_{LS}$, obtained from the total energy difference between the high- and low-spin states, respectively, whereas the term $P\Delta V$ accounts for thermal expansion, and ΔS_{ele} is the electronic entropy increment that arises from the differences in S and L. For the sake of completeness, we emphasize that isolated molecules account as well for energy and entropy variations due to rotation and translation, ΔS_{rot} and ΔS_{tra}, respectively, that usually are omitted in solid-state calculations. The two remaining contributions, ΔE_{vib} and ΔS_{vib}, can be obtained from the set of harmonic vibrational frequencies, $\{\nu\}$, by means of the vibrational temperature $\theta_{vib} = h\nu_i/k_B$, for all $\nu_i \in \{\nu\}$, through the expressions

$$E_{vib} = N_A k_B \sum_{\{\nu\}} \left(\frac{\theta_{vib}}{2} + \frac{\theta_{vib}}{e^{\theta_{vib}/T} - 1} \right) \quad (4)$$

$$S_{vib} = N_A k_B \sum_{\{\nu\}} \left(\frac{\theta_{vib}/T}{e^{\theta_{vib}/T} - 1} - \ln[1 - e^{\theta_{vib}/T}] \right) \quad (5)$$

The degrees of freedom included explicitly are illustrated in Figure 1. They are a subset of the total $\{\nu\}$, chosen under the assumption that contributions to E_{vib} and S_{vib} from the difference between the outermost atoms roughly cancel between the spin states. For the dispersion corrected computations, PBE(D3) + U_{eff}, only the first coordination shell surrounding the metallic centers, was considered due to computing resource limitations.

We also performed CASSCF[62,63] calculations with the ORCA electronic structure package[64] to confirm the axial zero-field splitting (ZFS) parameter, D, in eq 6 below. Reliable determination of the sign of D is a key issue because there is no experimental insight about that for the Cr^{III} case. For the ORCA calculations, we used the def2-QZVP basis set with the def2/JK and def2-QZVP/C auxiliary basis sets.[65−67] That choice was made to procure convergence of the spin Hamiltonian parameters with respect to the basis set. The active space was 3 electrons in 10 orbitals. The average energy from the lowest root with spin S = 3/2 and the lowest eight roots with spin S = 1/2 were minimized during the calculation, with all roots equally weighted. The spin−orbit interaction contribution was computed through the spin−orbit mean field

https://doi.org/10.1021/acs.jpca.4c06723
J. Phys. Chem. A 2024, 128, 10929−10935

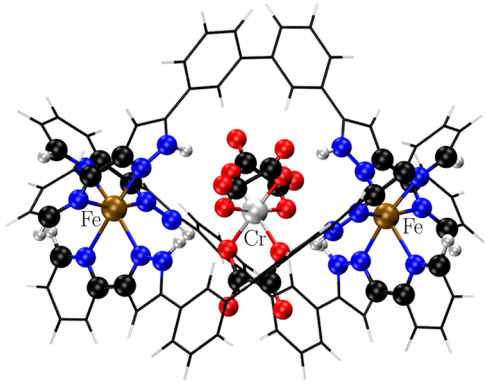

Figure 1. Schematic representation of the $[Cr(ox)_3]@[Fe_2L_3]^+$ cationic assembly. The atoms illustrated with spheres correspond to the choice of degrees of freedom used for the calculation of harmonic vibrational frequencies for PBE + U_{eff}, whereas a first coordination sphere approximation for each metallic center was considered for PBE(D3) + U_{eff}.

approximation[68] and the state interaction method.[69,70] The state interaction calculations relied on 80 low-energy spin−orbit states, originated from 10 spin-free roots with $S = 3/2$ and 20 with $S = 1/2$. We also added dynamical correlation beyond the active space using the NEVPT2 method[71] before including the spin−orbit interaction.

To describe the magnetic properties of the complexes that arise from the magnetic center interactions, we used the phenomenological spin Hamiltonian

$$\hat{H} = \sum_{i=1}^{2} J_{\{Cr/Fe\}^{III}Fe^{II},i}\hat{\mathbf{S}}_{\{Cr/Fe\}^{III}}\cdot\hat{\mathbf{S}}_{Fe^{II},i} + D(\hat{\mathbf{S}}_{\{Cr/Fe\}^{III}}\cdot\boldsymbol{e}_z)^2 + E[(\hat{\mathbf{S}}_{\{Cr/Fe\}^{III}}\cdot\boldsymbol{e}_x)^2 - (\hat{\mathbf{S}}_{\{Cr/Fe\}^{III}}\cdot\boldsymbol{e}_y)^2] \quad (6)$$

Here, $\hat{\mathbf{S}}_{\{Cr/Fe\}^{III}}$ is the spin for the Cr^{III} or Fe^{III} ion, while $\hat{\mathbf{S}}_{Fe^{II},i}$ is the spin for the first or second Fe^{II} ion. For them, the exchange coupling constant $J_{\{Cr/Fe\}^{III},Fe^{II}}$ corresponds to the interaction between the metal center of the SIM and the high-spin state of an Fe^{II} ion in the helicate moiety. Finally, $\boldsymbol{e}_x$, $\boldsymbol{e}_y$, and $\boldsymbol{e}_z$ are the orthonormal basis vectors of the so-called eigenframe for the local magnetic anisotropy on its axial and transversal components D and E, respectively.

For orderliness in the ensuing discussion, it is helpful to introduce the distinct labeling of different possible molecular states at this point. First, both experimental findings and computational evidence confirm what might be expected, namely, that the two Fe^{II} centers are essentially independent so far as spin switching is concerned. Therefore, one of the system states has both Fe^{II} in a low-spin state labeled LL. The labels LH and HH then correspond, respectively, to one Fe^{II} in the low-spin state, the other in the high-spin state, or both in high-spin state. Of course, there also are two types of relative spin orientations between the SIM and the crossover centers in the supramolecular complex, namely, parallel and antiparallel, FM and AFM, respectively, hereafter. The sign convention in eq 6 is that AFM corresponds to $J > 0$. We find no evidence of a system state for which the SIM is AFM with respect to one Fe^{II} and FM with respect to the other. Regarding the hypothetical HH state discussed below, the convention also holds.

Parametrization of the exchange coupling constant J, for the spin Hamiltonian in eq 6, was done by using the broken symmetry method. In general, the isotropic exchange coupling constant between a pair of magnetic centers can be calculated from the energy difference between two arbitrary low-energy states ψ_1 and ψ_2 with the relation

$$J = 2\frac{E(\psi_1) - E(\psi_2)}{\langle\hat{S}^2\rangle_{\psi_1} - \langle\hat{S}^2\rangle_{\psi_2}} \quad (7)$$

Here, $\hat{S}^2$ is the square of the total spin for the molecule. For the broken symmetry case, the FM and AFM states are mapped to the states $|\uparrow\uparrow\rangle \equiv |m_{s,1} = S_1, m_{s,2} = S_2\rangle$ and $|\uparrow\downarrow\rangle \equiv |m_{s,1} = S_1, m_{s,2} = -S_2\rangle$, respectively. In consequence, eq 7 reduces to $J = (E_{FM} - E_{AFM})/(2S_1S_2)$, an expression equivalent to Noodleman's original result, when $S_1 = S_2$.[72]

For a system with three or more magnetic centers which is characterized by multiple exchange coupling constants, eq 7 can be generalized into a set of linear equations. For these molecules in particular, we used a generalized methodology for noncollinear spins, mapping the state for the whole molecule to a single direct product of local spin states, each being high-spin with its own quantization axis. See the Appendix of ref 73. Definitions of the spin operators and matrices used there and here are accessible most readily in ref 74.

For the parameters D and E, on the other hand, we used the local dependence of the energy on a particular spin direction while keeping the remaining directions fixed.[75] These were characterized through the polar and azimuthal coordinates θ and ϕ, respectively, and were sampled uniformly using steps of $\pi/6$ radians on the unit sphere to form the set $\phi = 0$ and π rad, $\phi = \pi/2$ and $3\pi/2$ rad, and $\theta = \pi/2$ rad. We performed constrained Kohn−Sham calculations[76] for that set of spin rotations and then used those total energies to fit the ZFS parameters. In detail, the second-order ZFS Hamiltonian can be expressed as $\hat{H}_{ZFS} = \hat{\mathbf{S}}\cdot\boldsymbol{D}\cdot\hat{\mathbf{S}}$, where $\boldsymbol{D}$ is a 3×3 real symmetric tensor. It can be written in a diagonal form by changing the reference frame. With $\boldsymbol{D}$ diagonal, $\hat{H}_{ZFS} = D\hat{S}_z^2 + E(\hat{S}_x^2 - \hat{S}_y^2) + C$, with $D = D_{zz} - \frac{1}{2}(D_{xx} + D_{yy})$, and a constant energy shift to all energy levels, $C = \frac{1}{3}(D_{xx} + D_{yy} + D_{zz} - D)S(S+1)$, that can be omitted. Determination of the reference for which $\boldsymbol{D}$ is diagonal was done using the Kohn−Sham calculations to sample the grid of spin directions. The lowest-energy direction defines an easy axis, whereas the highest-energy direction defines an easy plane. We chose the easy axis as the local z axis. For the easy-plane anisotropy case, we chose the lowest- and highest-energy spin directions for the plane perpendicular to the local z axis as the local $x(y)$ and $y(x)$ directions, respectively. Note that such a choice follows the convention $0 < E/D < 1/3$.

RESULTS AND DISCUSSION

We begin by noting that for both complexes, the AFM pairing between the SIM and the bistable spin center, where a single Fe^{II} switches, is favored energetically. The magnitudes with respect to the FM pairing differ by 2.38(25) and 0.98(10) kJ mol^{-1} (meV) for $[Cr(ox)_3]@[Fe_2L_3]^+$ and $[Fe(ox)_3]@[Fe_2L_3]^+$, respectively. The first section of Table 2 provides the calculated ΔE_{HL} values for both systems for various possible cases. It is important to notice that due to the limited number of degrees of freedom for the calculation of the harmonic vibrational modes in E_{vib} and S_{vib}, as expressed in eqs 4 and 5, the computed $T_{1/2}$ values for both supramolecular complexes inevitably will be overestimated compared to experimental values, independent of the choice of magnetic

https://doi.org/10.1021/acs.jpca.4c06723
J. Phys. Chem. A 2024, 128, 10929−10935

Table 2. Calculated ΔE_{HL} Values, Including Zero-Point Energy Contributions for Various Configurations of $[Cr(ox)_3]@[Fe_2L_3]^+$ and $[Fe(ox)_3]@[Fe_2L_3]^+$, with the Associated Change in Enthalpy and Entropy at the Transition Temperature for Both PBE + U_{eff} and PBE(D3) + U_{eff} Density Functional Approximations, DFA[a]

		$[Cr(ox)_3]@[Fe_2L_3]^+$		$[Fe(ox)_3]@[Fe_2L_3]^+$	
thermodynamics	DFA + U_{eff}	FM	AFM	FM	AFM
ΔE_{HL}	PBE	28.64	26.26	30.79	29.81
	PBE(D3)	44.20	40.97	45.54	45.56
ΔH	PBE	26.24	24.07	28.46	27.36
	PBE(D3)	41.43	38.33	42.76	42.82
ΔS	PBE	75.26	18.22	69.47	78.15
	PBE(D3)	62.72	62.72	63.68	62.72
spin Hamiltonian		D	E	D	E
LL	PBE	−0.508	−0.016	0.137	0.000
	PBE(D3)	−0.629	−0.016	0.137	0.000
LH	PBE	−0.597	−0.040	0.137	0.008
	PBE(D3)	−0.678	−0.040	0.145	0.000
		$J_{Cr^{III},Fe^{II}}$		$J_{Fe^{III},Fe^{II}}$	
LH	PBE	0.315		0.290	
LH	PBE(D3)	0.218		0.306	

[a] ΔE_{HL}, ΔH, and ΔS are reported in units of kJ mol^{-1} and ΔS in J mol^{-1} K^{-1}. The spin Hamiltonian parameters D, E, and J are included as well and reported in units of cm^{-1}.

coupling. This is more evident for calculations with the PBE(D3) + U_{eff} approximation because they used only the first coordination shells for the respective metal centers.

Despite these limitations, the qualitative and semiquantitative relationships should be valid. In detail, the calculated $T_{1/2}$ for the AFM coupling is 320 and 350 K for $[Cr(ox)_3]@[Fe_2L_3]^+$ and $[Fe(ox)_3]@[Fe_2L_3]^+$, respectively, while for the FM case, the values are 350 and 410 K, respectively. The counterparts for PBE(D3) + U_{eff} results are 609 and 680 K for the AFM coupling but 664 and 675 K for the FM interaction. In comparison, the experimental values are ≈200 and 250−400 K,[44,45] respectively. It is noticeable that the $\Delta T_{1/2}$ between the parallel and antiparallel couplings for the assembly with the Fe^{III} moiety is twice that of the Cr^{III} one for PBE + U_{eff}, but these findings are not transferable to the PBE(D3) + U_{eff} results due to the limited degrees of freedom used in the latter calculations. This observation, when paired with the energy differences observed for both couplings, suggests that the bistable center and SIM in the $[Cr(ox)_3]@[Fe_2L_3]^+$ complex are preferably antiparallel, whereas for $[Fe(ox)_3]@[Fe_2L_3]^+$, this preference is small enough to allow competition between the FM and AFM interactions during the spin transition. For the sake of completeness, Table 2 provides a comparison of the ΔH and ΔS contributions calculated at $T_{1/2}$ for both spin pairings. The results indicate that ΔH for the FM pairing is larger than that for the AFM interaction for both molecules, except for $[Cr(ox)_3]@[Fe_2L_3]^+$. In it, the AFM coupling essentially is the same for PBE(D3) + U_{eff}, but we reiterate that such an observation is limited by the reduced contributions to ΔE_{vib} and ΔS_{vib}.

With the calculation of the relevant low- and high-spin energetics in hand and the finding that they are in at least semiquantitative agreement with experiment, spin Hamiltonian parametrization follows. We begin with the ZFS parameters.

Table 3 shows that the spin−orbit interaction dominates over the spin−spin dipolar contribution for the low-spin state

Table 3. Zero-Field Splitting Parameters D and E for the Low-Spin States of $[Cr(ox)_3]@[Fe_2L_3]^+$ and $[Fe(ox)_3]@[Fe_2L_3]^+$ [a]

	$[Cr(ox)_3]@[Fe_2L_3]^+$		$[Fe(ox)_3]@[Fe_2L_3]^+$	
	D	E	D	E
spin−orbit	−0.508	−0.016	0.137	0.000
spin−spin	−0.121	−0.000	−0.008	0.000
total	−0.629	−0.016	0.129	0.000
ref	−0.669[b]	0−0.105[c]	0.121[c]	0.032[c]

[a] All quantities are reported for PBE + U_{eff} in units of cm^{-1}. [b] Result from CASSCF calculation. [c] Obtained from ref 45.

in both complexes. Particularly, both the spin−spin and spin−orbit interactions give negative contributions to D for Cr^{III}, with the spin−orbit interaction contribution being roughly 81% of the total value of D = −0.629 cm^{-1} (−0.078 meV). The CASSCF result, D = −0.669 cm^{-1} (−0.083 meV), agrees quite well in both magnitude and sign. Those magnitudes agree well with an experimental range 0.637−0.774 cm^{-1} (0.079−0.096 meV)[77] but with the opposite sign. Plausibly, the sign discrepancy is traceable to the different physical and chemical environment for the $[Cr(ox)_3]^{3-}$ moiety in the experiment.

For the Fe^{III} ion system, Table 3 shows that the spin−orbit and spin−spin interactions have opposite signs. The spin−spin interaction accounts for only ≈6% of the calculated total value of D = 0.129 cm^{-1} (0.016 meV). These results match the experimental values[45] and confirm that the two complexes are quantitatively and qualitatively distinct.

The second section in Table 2 reports the parametrization for the LL and LH states. Only the spin−orbit contribution to the ZFS parameters is shown. Obviously, in both LL systems, the exchange coupling constant J = 0. More interestingly, for the LH case, both $J_{Cr^{III}-Fe^{II}}$ and $J_{Fe^{III}-Fe^{II}}$ are positive, denoting AFM coupling. They differ by only 2.5 × 10^{-2} cm^{-1} (3 × 10^{-3} meV), in agreement with our findings for the lower transition temperature calculated for both coordination assemblies with antiparallel interaction.

The axial ZFS parameter for Cr^{III} reported in both Tables 2 and 3 is negative, clear evidence for an easy-axis magnetic anisotropy located along the 3-fold rotational symmetry axis of the $[Cr(ox)_3]^{3-}$ moiety. The positive sign for Fe^{III} indicates, in contrast, the presence of a magnetic easy plane that is perpendicular to the 3-fold rotational symmetry axis of the $[Fe(ox)_3]^{3-}$ moiety. Results in Table 3 also show that the magnitude of D for Cr^{III} is sensitive to the state of spin-crossover Fe^{II}. That is, D increases by nearly 13% when the Fe^{II} switches from LS to HS. Corresponding behavior is not observed for Fe^{III}, which is nearly insensitive to the spin-switching behavior of the Fe^{II} moiety. These results agree with the experimental findings for the coherence suppression found for $[Fe(ox)_3]@[Fe_2L_3]^+$.[45]

It also is of interest that the values of the transverse component of the magnetic anisotropy, E, in Table 3, are on the order of 10^{-2} cm^{-1} (10^{-3} meV) and share the same sign as their axial counterparts D. Nonetheless, their magnitudes are sufficiently small that we can neglect the E contribution in eq 6. Note that the magnitudes are about as small as the convergence tolerance for the energy in the self-consistent field.

https://doi.org/10.1021/acs.jpca.4c06723
J. Phys. Chem. A 2024, 128, 10929−10935

Finally, we considered the HH state of $[Cr(ox)_3]@[Fe_2L_3]^+$. Though it has not been observed experimentally, it is accessible computationally. The magnitudes of D and E are reported in Table 4. Additionally, data in Table 4 show that the exchange couplings between the Cr^{III} ion and the Fe^{II} ions are sizable and of AFM type, with $J_{\{Cr/Fe\}^{III},Fe^{II}}$ for an interatomic distance of 5.08 Å, about 4 times larger than that for the interatomic distance of 5.35 Å.

Table 4. Spin Hamiltonian Parameters due to the Spin−Orbit Interaction for the HH Spin State of $[Cr(ox)_3]@[Fe_2L_3]^+$ [a]

	magnitude	
parameter	PBE + U_{eff} geometry	PBE geometry
$D_{Cr^{III}}$ [b]	−0.702	−0.758
$E_{Cr^{III}}$ [c]	−0.032	−0.016
$J_{Cr^{III},Fe^{II}}$	0.065 [d]	0.097 [e]
$J_{Cr^{III},Fe^{II}}$	0.355 [f]	0.363 [g]
$D_{Fe^{II}}$	−4.573	−4.686
$E_{Fe^{II}}$	−0.871	−0.815
$J_{Fe^{II},Fe^{II}}$	0.016	0.000

[a]All values are reported for PBE + U_{eff} and in units of cm^{-1}. [b]Experimental value of 0.637−0.774 from ref 77. [c]Experimental value of 0.000−0.105 from ref 77. [d]d = 5.35 Å. [e]d = 5.29 Å. [f]d = 5.08 Å. [g]d = 5.11 Å.

Results to here are based on molecular geometries as relaxed by the PBE + U_{eff} method with the aforementioned finite U_{eff} values. To assess robustness, we also relaxed the molecular geometries without the Hubbard-U_{eff} correction for all of the spin states and recalculated the spin Hamiltonian parameters with finite U values. All conclusions on the spin Hamiltonian parameters remain valid. Most spin Hamiltonian parameters change by a few microelectron volts, which can be treated as numerical errors. A comparison of the HH state of $[Cr(ox)_3]@[Fe_2L_3]^+$ is given in Table 4. The difference is a direct consequence of the two Fe^{II} interion distances with respect to the Cr^{III} center. The exchange coupling constant between the two Fe^{II} ions is essentially zero, which is not a surprise, given the distance between those two centers. Our calculations show that the HS Fe^{II} ion has easy-axis magnetic anisotropy and that its in-plane magnetic anisotropy is high. The thermodynamic analysis resulted in a spin-switching energy of 29.27 kJ mol^{-1} that is associated with a transition temperature of approximately 490 K, with ΔH = 26.90 kJ mol^{-1} (272.8 meV) and ΔS = 54.03 J mol^{-1} K^{-1} (0.56 meV K^{-1}). These results suggest that it might be worthwhile to investigate the possibility of observing the HH state experimentally, although the oxalate group will probably start decomposing at that temperature.

CONCLUSIONS

We have provided careful DFT + U_{eff} calculations for the structure and energetics of different spin states for the $\{Cr/Fe\}^{III}$ SIM embedded in a spin-crossover system. This includes calculations of the transition temperature that are in reasonable agreement with the experiment. From those calculated results, we parametrized a spin Hamiltonian for each system. Both are found to be antiparallel with respect to the ordering between the crossover and single-ion magnet subsystems. The $[Cr(ox)_3]@[Fe_2L_3]^+$ system is of easy-axis type, while the $[Fe(ox)_3]@[Fe_2L_3]^+$ system is of easy plane. That distinction is consistent with the experimental results for decoherence in $[Fe(ox)_3]@[Fe_2L_3]^+$.[45] Results for the hypothetical $[Cr(ox)_3]@[Fe_2L_3]^+$ with both Fe^{II} in a high-spin state may provide a basis for the experimental search. However, the crossover energy is 3 kJ mol^{-1} (30 meV) larger than that for the experimental species with one high-spin Fe^{II} ion, and the high transition temperature of nearly 490 K can decompose the Cr^{III} moiety.

ASSOCIATED CONTENT

Supporting Information

The Supporting Information is available free of charge at https://pubs.acs.org/doi/10.1021/acs.jpca.4c06723.

Input example for VASP and the optimized Cartesian coordinates for all species considered in this work (TXT)

AUTHOR INFORMATION

Corresponding Authors

Richard G. Hennig − *Center for Molecular Magnetic Quantum Materials, University of Florida, Gainesville, Florida 32611, United States; Department of Materials Science and Engineering, University of Florida, Gainesville, Florida 32611, United States;* orcid.org/0000-0003-4933-7686; Email: rhennig@ufl.edu

S. B. Trickey − *Center for Molecular Magnetic Quantum Materials, University of Florida, Gainesville, Florida 32611, United States; Department of Physics and Department of Chemistry, University of Florida, Gainesville, Florida 32611, United States;* orcid.org/0000-0001-9224-6304; Email: trickey@ufl.edu

Authors

Angel Albavera-Mata − *Center for Molecular Magnetic Quantum Materials, University of Florida, Gainesville, Florida 32611, United States; Department of Materials Science and Engineering, University of Florida, Gainesville, Florida 32611, United States;* orcid.org/0000-0003-1521-678X

Shuanglong Liu − *Center for Molecular Magnetic Quantum Materials, University of Florida, Gainesville, Florida 32611, United States; Department of Physics, Northeastern University, Boston, Massachusetts 02115, United States;* orcid.org/0000-0003-3253-5491

Hai-Ping Cheng − *Center for Molecular Magnetic Quantum Materials, University of Florida, Gainesville, Florida 32611, United States; Department of Physics, Northeastern University, Boston, Massachusetts 02115, United States;* orcid.org/0000-0001-5990-1725

Complete contact information is available at: https://pubs.acs.org/10.1021/acs.jpca.4c06723

Notes

The authors declare no competing financial interest.

ACKNOWLEDGMENTS

This work was supported as part of the Center for Molecular Magnetic Quantum Materials, an Energy Frontier Research Center funded by the U.S. Department of Energy, Office of Science, Basic Energy Sciences under Award No. DE-SC0019330. This research used resources of the National Energy Research Scientific Computing Center (NERSC), a

Department of Energy Office of Science User Facility using NERSC award BES-ERCAP0022828.

REFERENCES

(1) Leuenberger, M. N.; Loss, D. Quantum computing in molecular magnets. *Nature* **2001**, *410*, 789−793.
(2) Troiani, F.; Ghirri, A.; Affronte, M.; Carretta, S.; Santini, P.; Amoretti, G.; Piligkos, S.; Timco, G.; Winpenny, R. E. P. Molecular Engineering of Antiferromagnetic Rings for Quantum Computation. *Phys. Rev. Lett.* **2005**, *94*, No. 207208.
(3) Ardavan, A.; Rival, O.; Morton, J. J. L.; Blundell, S. J.; Tyryshkin, A. M.; Timco, G. A.; Winpenny, R. E. P. Will Spin-Relaxation Times in Molecular Magnets Permit Quantum Information Processing? *Phys. Rev. Lett.* **2007**, *98*, No. 057201.
(4) Luis, F.; Repollés, A.; Martínez-Pérez, M. J.; et al. Molecular Prototypes for Spin-Based CNOT and SWAP Quantum Gates. *Phys. Rev. Lett.* **2011**, *107*, No. 117203.
(5) Vincent, R.; Klyatskaya, S.; Ruben, M.; Wernsdorfer, W.; Balestro, F. Electronic read-out of a single nuclear spin using a molecular spin transistor. *Nature* **2012**, *488*, 357−360.
(6) Bader, K.; Dengler, D.; Lenz, S.; Endeward, B.; Jiang, S.-D.; Neugebauer, P.; van Slageren, J. Room temperature quantum coherence in a potential molecular qubit. *Nat. Commun.* **2014**, *5*, No. 5304.
(7) Fataftah, M. S.; Zadrozny, J. M.; Rogers, D. M.; Freedman, D. E. A Mononuclear Transition Metal Single-Molecule Magnet in a Nuclear Spin-Free Ligand Environment. *Inorg. Chem.* **2014**, *53*, 10716−10721.
(8) Zadrozny, J. M.; Niklas, J.; Poluektov, O. G.; Freedman, D. E. Millisecond Coherence Time in a Tunable Molecular Electronic Spin Qubit. *ACS Cent. Sci.* **2015**, *1*, 488−492.
(9) Shiddiq, M.; Komijani, D.; Duan, Y.; Gaita-Ariño, A.; Coronado, E.; Hill, S. Enhancing coherence in molecular spin qubits via atomic clock transitions. *Nature* **2016**, *531*, 348−351.
(10) Ruster, T.; Schmiegelow, C. T.; Kaufmann, H.; Warschburger, C.; Schmidt-Kaler, F.; Poschinger, U. G. A long-lived Zeeman trapped-ion qubit. *Appl. Phys. B: Lasers Opt.* **2016**, *122*, No. 254.
(11) Jenkins, M. D.; Duan, Y.; Diosdado, B.; García-Ripoll, J. J.; Gaita-Ariño, A.; Giménez-Saiz, C.; Alonso, P. J.; Coronado, E.; Luis, F. Coherent manipulation of three-qubit states in a molecular single-ion magnet. *Phys. Rev. B* **2017**, *95*, No. 064423.
(12) Gaita-Ariño, A.; Luis, F.; Hill, S.; Coronado, E. Molecular spins for quantum computation. *Nat. Chem.* **2019**, *11*, 301−309.
(13) Martínez-Pérez, M. J.; Cardona-Serra, S.; Schlegel, C.; et al. Gd-Based Single-Ion Magnets with Tunable Magnetic Anisotropy: Molecular Design of Spin Qubits. *Phys. Rev. Lett.* **2012**, *108*, No. 247213.
(14) Woodruff, D. N.; Winpenny, R. E. P.; Layfield, R. A. Lanthanide Single-Molecule Magnets. *Chem. Rev.* **2013**, *113*, 5110−5148.
(15) Graham, M. J.; Zadrozny, J. M.; Shiddiq, M.; Anderson, J. S.; Fataftah, M. S.; Hill, S.; Freedman, D. E. Influence of Electronic Spin and Spin−Orbit Coupling on Decoherence in Mononuclear Transition Metal Complexes. *J. Am. Chem. Soc.* **2014**, *136*, 7623−7626.
(16) Gómez-Coca, S.; Aravena, D.; Morales, R.; Ruiz, E. Large magnetic anisotropy in mononuclear metal complexes. *Coord. Chem. Rev.* **2015**, *289*−*290*, 379−392.
(17) Bar, A. K.; Pichon, C.; Sutter, J.-P. Magnetic anisotropy in two- to eight-coordinated transition−metal complexes: Recent developments in molecular magnetism. *Coord. Chem. Rev.* **2016**, *308*, 346−380.
(18) Dobrovitski, V. V.; Katsnelson, M. I.; Harmon, B. N. Mechanisms of Decoherence in Weakly Anisotropic Molecular Magnets. *Phys. Rev. Lett.* **2000**, *84*, 3458.
(19) Mirzoyan, R.; Kazmierczak, N. P.; Hadt, R. G. Deconvolving Contributions to Decoherence in Molecular Electron Spin Qubits: A Dynamic Ligand Field Approach. *Chem. - Eur. J.* **2021**, *27*, 9482.
(20) Harman, W. H.; Harris, T. D.; Freedman, D. E.; et al. Slow Magnetic Relaxation in a Family of Trigonal Pyramidal Iron(II) Pyrrolide Complexes. *J. Am. Chem. Soc.* **2010**, *132*, 18115−18126.
(21) Frost, J. M.; Harriman, K. L. M.; Murugesu, M. The rise of 3-d single-ion magnets in molecular magnetism: towards materials from molecules? *Chem. Sci.* **2016**, *7*, 2470−2491.
(22) Yue, Y.; Yan, P.; Sun, J.; Li, G. Single molecule magnet of 2D Salen-type dysprosium coordination polymer. *Inorg. Chem. Commun.* **2015**, *54*, 5−8.
(23) Vallejo, J.; Fortea-Pérez, F. R.; Pardo, E.; Benmansour, S.; Castro, I.; Krzystek, J.; Armentano, D.; Cano, J. Guest-dependent single-ion magnet behaviour in a cobalt(II) metal−organic framework. *Chem. Sci.* **2016**, *7*, 2286−2293.
(24) Liu, K.; Zhang, X.; Meng, X.; Shi, W.; Chengab, P.; Powell, A. K. Constraining the coordination geometries of lanthanide centers and magnetic building blocks in frameworks: a new strategy for molecular nanomagnets. *Chem. Soc. Rev.* **2016**, *45*, 2423−2439.
(25) Zhang, S.; Li, H.; Duan, E.; Han, Z.; Li, L.; Tang, J.; Shi, W.; Cheng, P. A 3D Heterometallic Coordination Polymer Constructed by Trimeric {NiDy2} Single-Molecule Magnet Units. *Inorg. Chem.* **2016**, *55*, 1202−1207.
(26) Yue, Y.; Hou, G.; Yao, X.; Li, G. Single molecular magnet of lanthanide coordination polymer with 1D helical-like chain based on flexible Salen-type ligand. *Polyhedron* **2017**, *129*, 157−163.
(27) Rigamonti, L.; Vaccari, M.; Roncaglia, F.; Baschieri, C.; Forni, A. New Silver(I) Coordination Polymer with Fe_4 Single-Molecule Magnets as Long Spacer. *Magnetochemistry* **2018**, *4*, 43.
(28) Coronado, E. Molecular magnetism: from chemical design to spin control in molecules, materials and devices. *Nat. Rev. Mater.* **2020**, *5*, 87−104.
(29) Houard, F.; Gendron, F.; Suffren, Y.; et al. Single-chain magnet behavior in a finite linear hexanuclear molecule. *Chem. Sci.* **2021**, *12*, 10613−10621.
(30) Aulakh, D.; Pyser, J. B.; Zhang, X.; Yakovenko, A. A.; Dunbar, K. R.; Wriedt, M. Metal−Organic Frameworks as Platforms for the Controlled Nanostructuring of Single-Molecule Magnets. *J. Am. Chem. Soc.* **2015**, *137*, 9254−9257.
(31) Zhang, X.; Vieru, V.; Feng, X.; et al. Influence of Guest Exchange on the Magnetization Dynamics of Dilanthanide Single-Molecule-Magnet Nodes within a Metal−Organic Framework. *Angew. Chem., Int. Ed.* **2015**, *54*, 9861−9865.
(32) Mon, M.; Pascual-Álvarez, A.; Grancha, T.; Cano, J.; Ferrando-Soria, J.; Lloret, F.; Gascon, J.; Pasán, J.; Armentano, D.; Pardo, E. Solid-State Molecular Nanomagnet Inclusion into a Magnetic Metal−Organic Framework: Interplay of the Magnetic Properties. *Chem. - Eur. J.* **2016**, *22*, 539−545.
(33) Aulakh, D.; Xie, H.; Shen, Z.; Harley, A.; Zhang, X.; Yakovenko, A. A.; Dunbar, K. R.; Wriedt, M. Systematic Investigation of Controlled Nanostructuring of Mn_{12} Single-Molecule Magnets Templated by Metal−Organic Frameworks. *Inorg. Chem.* **2017**, *56*, 6965−6972.
(34) Liu, T.; Fan, Z.; Mi, Z.; Du, W.; Song, X.; Liu, R.; Wang, H.; Du, Y. Metal organic frameworks as platforms for the nanostructuring of Mn_3 single molecule magnets. *J. Solid State Chem.* **2022**, *305*, No. 122697.
(35) Erler, P.; Schmitt, P.; Barth, N.; Irmler, A.; Bouvron, S.; Huhn, T.; Groth, U.; Pauly, F.; Gragnaniello, L.; Fonin, M. Highly Ordered Surface Self-Assembly of Fe_4 Single Molecule Magnets. *Nano Lett.* **2015**, *15*, 4546−4552.
(36) Inose, T.; Tanaka, D.; Ivasenko, O.; Tahara, K.; Feyter, S. D.; Tobe, Y.; Tanaka, H.; Ogawa, T. Coadsorption of Tb^{III}-Porphyrin Double-decker Single-molecule Magnets in a Porous Molecular Network: Toward Controlled Alignment of Single-molecule Magnets on a Carbon Surfac. *Chem. Lett.* **2016**, *45*, 286−288.
(37) Baltic, R.; Pivetta, M.; Donati, F.; Wäckerlin, C.; Singha, A.; Dreiser, J.; Rusponi, S.; Brune, H. Superlattice of Single Atom Magnets on Graphene. *Nano Lett.* **2016**, *16*, 7610−7615.

https://doi.org/10.1021/acs.jpca.4c06723
J. Phys. Chem. A 2024, 128, 10929−10935

(38) Poggini, L.; Tancini, E.; Danieli, C.; et al. Engineering Chemisorption of Fe_4 Single-Molecule Magnets on Gold. *Adv. Mater. Interfaces* **2021**, *8*, No. 2101182.
(39) Mannini, M.; Pineider, F.; Sainctavit, P.; et al. Magnetic memory of a single-molecule quantum magnet wired to a gold surface. *Nat. Mater.* **2009**, *8*, 194−197.
(40) Feng, X.; Mathonière, C.; Jeon, I.-R.; Rouzières, M.; Ozarowski, A.; Aubrey, M. L.; Gonzalez, M. I.; Clérac, R.; Long, J. R. Tristability in a Light-Actuated Single-Molecule Magnet. *J. Am. Chem. Soc.* **2013**, *135*, 15880−15884.
(41) Hao, H.; Zheng, X.; Jia, T.; Zeng, Z. Room temperature memory device using single-molecule magnets. *RSC Adv.* **2015**, *5*, 54667−54671.
(42) Ma, Y.-J.; Hu, J.-X.; Han, S.-D.; Pan, J.; Li, J.-H.; Wang, G.-M. Manipulating On/Off Single-Molecule Magnet Behavior in a Dy(III)-Based Photochromic Complex. *J. Am. Chem. Soc.* **2020**, *142*, 2682−2689.
(43) Xue, H.-B.; Liang, J.-Q.; Liu, W.-M. Manipulation and readout of spin states of a single-molecule magnet by a spin-polarized current. *Phys. E* **2022**, *138*, No. 115086.
(44) Darawsheh, M.; Barrios, L. A.; Roubeau, O.; Teat, S. J.; Aromí, G. Encapsulation of a Cr^{III} Single-Ion Magnet within an Fe^{II} Spin-Crossover Supramolecular Host. *Angew. Chem.* **2018**, *130*, 13697−13701.
(45) Barrios, L. A.; Diego, R.; Darawsheh, M.; Martínez, J. I.; Roubeau, O.; Aromí, G. A ferric guest inside a spin crossover ferrous helicate. *Chem. Commun.* **2022**, *58*, 5375−5378.
(46) Barrios, L. A.; Teat, S. J.; Roubeau, O.; Aromí, G. A Supramolecular Helicate with Two Independent Fe(II) Switchable Centres and a $[Fe(anilate)_3]^{3-}$ Guest. *Chem. Commun.* **2023**, *59*, 10628−10631.
(47) McWeeny, R.; Mizuno, Y. The density matrix in many-electron quantum mechanics II. Separation of space and spin variables; spin coupling problems. *Proc. R. Soc. London, Ser. A* **1961**, *259*, 554−557.
(48) McWeeny, R. *Spins in Chemistry, Current Chemical Concepts*; Academic Press: New York, 1970.
(49) Harriman, J. E. *Theoretical Foundations of Electron Spin Resonance*; Academic Press: London, 1978.
(50) Neese, F.; Solomon, E. I. Calculation of Zero-Field Splittings, g-Values, and the Relativistic Nephelauxetic Effect in Transition Metal Complexes. Application to High-Spin Ferric Complexes. *Inorg. Chem.* **1998**, *37*, 6568−6582.
(51) Pederson, M. R.; Khanna, S. N. Magnetic anisotropy barrier for spin tunneling in Mn12O12 molecules. *Phys. Rev. B* **1999**, *60*, 9566.
(52) Reviakine, R.; Arbuznikov, A. V.; Tremblay, J.-C.; Remenyi, C.; Malkina, O. L.; Malkin, V. G.; Kaupp, M. Calculation of zero-field splitting parameters: Comparison of a two-component noncolinear spin-density-functional method and a one-component perturbational approach. *J. Chem. Phys.* **2006**, *125*, No. 054110.
(53) Chibotaru, L. F.; Ungur, L. Ab initio calculation of anisotropic magnetic properties of complexes. I. Unique definition of pseudospin Hamiltonians and their derivation. *J. Chem. Phys.* **2012**, *137*, No. 064112.
(54) Xiang, H.; Lee, C.; Koo, H.-J.; Gong, X.; Whangbo, M.-H. Magnetic properties and energy-mapping analysis. *Dalton Trans.* **2013**, *42*, 823−853.
(55) Kresse, G.; Furthmüller, J. Efficient iterative schemes for *ab initio* total-energy calculations using a plane-wave basis set. *Phys. Rev. B* **1996**, *54*, No. 11169.
(56) Perdew, J. P.; Burke, K.; Ernzerhof, M. Generalized Gradient Approximation Made Simple. *Phys. Rev. Lett.* **1996**, *77*, 3865.
(57) Perdew, J. P.; Burke, K.; Ernzerhof, M. Generalized Gradient Approximation Made Simple [Phys. Rev. Lett. 77, 3865 (1996)]. *Phys. Rev. Lett.* **1997**, *78*, 1396.
(58) Grimme, S.; Ehrlich, S.; Goerigk, L. Effect of the damping function in dispersion corrected density functional theory. *J. Comput. Chem.* **2011**, *32*, 1456.
(59) Cococcioni, M.; de Gironcoli, S. Linear Response Approach to the Calculation of the Effective Interaction Parameters in the LDA+U Method. *Phys. Rev. B* **2005**, *71*, No. 035105.
(60) Albavera-Mata, A.; Trickey, S. B.; Hennig, R. Mean Value Ensemble Hubbard-U Correction for Spin-Crossover Molecules. *J. Phys. Chem. Lett.* **2022**, *13*, 12049−12054.
(61) Mugiraneza, S.; Hallas, A. M. Tutorial: a beginner's guide to interpreting magnetic susceptibility data with the Curie-Weiss law. *Commun. Phys.* **2022**, *5*, No. 95.
(62) Siegbahn, P. E.; Heiberg, A.; Roos, B. O.; Levy, B. A Comparison of the Super-CI and the Newton-Raphson Scheme in the Complete Active Space SCF Method. *Phys. Scr.* **1980**, *21*, 323.
(63) Roos, B. O.; Taylor, P. R.; Siegbahn, P. E. A complete active space SCF method (CASSCF) using a density matrix formulated super-CI approach. *Chem. Phys.* **1980**, *48*, 157−173.
(64) Neese, F.; Wennmohs, F.; Becker, U.; Riplinger, C. The ORCA quantum chemistry program package. *J. Chem. Phys.* **2020**, *152*, No. 224108.
(65) Weigend, F.; Ahlrichs, R. Balanced basis sets of split valence, triple zeta valence and quadruple zeta valence quality for H to Rn: Design and assessment of accuracy. *Phys. Chem. Chem. Phys.* **2005**, *7*, 3297−3305.
(66) Weigend, F. Hartree-Fock exchange fitting basis sets for H to Rn. *J. Comput. Chem.* **2008**, *29*, 167−175.
(67) Hellweg, A.; Hättig, C.; Höfener, S.; Klopper, W. Optimized accurate auxiliary basis sets for RI-MP2 and RI-CC2 calculations for the atoms Rb to Rn. *Theor. Chem. Acc.* **2007**, *117*, 587−597.
(68) Neese, F. Efficient and accurate approximations to the molecular spin-orbit coupling operator and their use in molecular g-tensor calculations. *J. Chem. Phys.* **2005**, *122*, No. 034107.
(69) Malmqvist, P.-Å.; Roos, B. O. The CASSCF state interaction method. *Chem. Phys. Lett.* **1989**, *155*, 189−194.
(70) Malmqvist, P. k.; Roos, B. O.; Schimmelpfennig, B. The restricted active space (RAS) state interaction approach with spin−orbit coupling. *Chem. Phys. Lett.* **2002**, *357*, 230−240.
(71) Angeli, C.; Cimiraglia, R.; Evangelisti, S.; Leininger, T.; Malrieu, J. P. Introduction of n-electron valence states for multi-reference perturbation theory. *J. Chem. Phys.* **2001**, *114*, 10252−10264.
(72) Noodleman, L. Valence bond description of antiferromagnetic coupling in transition metal dimers. *J. Chem. Phys.* **1981**, *74*, 5737−5743.
(73) Yu, J.-X.; Chen, J.; Sullivan, N.; Cheng, H.-P. Dzyaloshinskii-Moriya interaction induced magnetoelectric coupling in a tetrahedral molecular spin-frustrated system. *Phys. Rev. B* **2022**, *106*, No. 054412.
(74) Stoll, S.; Schweiger, A. EasySpin, a comprehensive software package for spectral simulation and analysis in EPR. *J. Magn. Reson.* **2006**, *178*, 42−55.
(75) Yazback, M.; Liu, S.; Shatruk, M.; Christou, G.; Cheng, H.-P. Search for Toroidal Ground State and Magnetoelectric Effects in Molecular Spin Triangles with Antiferromagnetic Exchange. *J. Phys. Chem. A* **2023**, *127*, 3814−3823.
(76) Steiner, S.; Khmelevskyi, S.; Marsmann, M.; Kresse, G. Calculation of the magnetic anisotropy with projected-augmented-wave methodology and the case study of disordered $Fe_{1-x}Co_x$ alloys. *Phys. Rev. B* **2016**, *93*, 22.
(77) Husein Mor, H.; Weihe, H.; Bendix, J. Fitting of EPR spectra: The importance of a flexible bandwidth. *J. Magn. Reson.* **2010**, *207*, 283−286.

https://doi.org/10.1021/acs.jpca.4c06723
J. Phys. Chem. A 2024, 128, 10929−10935